



Relationship between mineralization kinetics and mechanistic pathway during malic acid photodegradation

Wenny Irawaty, Donia Friedmann, Jason Scott, Rose Amal*

ARC Centre of Excellence for Functional Nanomaterials, School of Chemical Engineering, The University of New South Wales, Sydney, NSW 2052, Australia

ARTICLE INFO

Article history:

Received 5 July 2010

Received in revised form 29 October 2010

Accepted 14 November 2010

Available online 2 December 2010

Keywords:

Malic acid

Photooxidation

Kinetics

Mineralization profile

Mechanism

ABSTRACT

The photocatalytic degradation of malic acid was studied under ambient conditions in an aqueous TiO₂ suspension. The results demonstrated the presence of four distinct mineralization rate variations over the course of its degradation. Differences in the mineralization rate were governed by the dominant intermediate present in the solution at that time. Initial mineralization was rapid (~175 μg C/min) resulting from the swift extraction of a carbon from strongly adsorbed malic acid via the photo-Kolbe mechanism. The mineralization rate then slowed down (~50–70 μg C/min) with the continued formation of an intermediate product (believed to be malonaldehydic acid), malonic acid and acetic acid in the solution. The findings provide greater insight into the photocatalytic degradation mechanism, illustrating the importance of intermediates and their attributes in relation to the overall rate of organic removal.

© 2010 Elsevier B.V. All rights reserved.

1. Introduction

TiO₂ photocatalytic oxidation of organic pollutants in an aqueous phase system has the potential to be solar driven and since it can completely mineralize organic pollutants it may prove to be ecologically and economically sustainable [1–3]. A quantification of the reaction kinetics and insight into the degradation mechanism of organics in aqueous environments are important in the application and process control of water treatment facilities [1,4,5]. Additionally, as reactions proceed in a stepwise fashion, the properties of the intermediates that are formed affect the reaction kinetics [6,7].

In heterogeneous photocatalysis, complexities arise due to the relationship between organic structure, photocatalyst surface properties, reaction environment and the resulting adsorption/desorption processes and their subsequent impact on the reaction kinetics [8–11]. Monitoring the overall mineralization rate has been of considerable interest to study photocatalytic reaction rates. However, mechanistic studies are often not anticipated in such reaction kinetic studies. In large-scale industrial applications, the degradation of some organics can be hindered during the water treatment process due to the formation of problematic intermediates, affecting the total treatment time required to achieve a desired water quality. Understanding which intermediate products are problematic and at what stage of the reaction they are formed is important.

Identifying those intermediates during the photocatalytic reaction is useful firstly for anticipating a slow down in the reaction and secondly, it provides an opportunity to alleviate their presence by simply adjusting the system pH for example. Other related aspects also relevant to these discussions are factors that influence the selectivity of photocatalytic reactions and why certain pathways are favored under certain conditions. This is relevant when comparing between photocatalytic systems whereby slightly different mixtures of intermediates and products are observed for the same parent compounds due to slight changes in the photocatalytic systems and experimental conditions [12,13]. In addition, information on the generation of strongly adsorbing intermediates during photocatalytic degradation reactions is often lacking since analytical tools often allow the detection of intermediates in solution and not on the photocatalyst surface. Thus ambiguities in mechanistic studies in systems involving strong adsorbates can arise. To this end, a better understanding of the photocatalysis degradation mechanisms of organic compounds is crucial.

In this study, the photocatalytic oxidation of malic acid (HOOCCH₂CHOHCOOH) was studied in an illuminated aqueous suspension of TiO₂ at ambient temperature and pressure. Malic acid is an interesting compound that undergoes a series of distinct decarboxylation steps during its degradation. The photocatalytic degradation of malic acid was first reported by Herrmann et al. [12]. The authors focused on deriving the photocatalytic degradation pathway of this acid. Danion et al. [13] studied the mineralization of malic acid using an optical fiber reactor. This latter study focused on assessing the photonic efficiency of the reaction. In our study, we focus on the mineralization rate profile of malic acid. We examine

* Corresponding author. Tel.: +61 2 9385 4361; fax: +61 2 9385 5966.
E-mail address: r.amal@unsw.edu.au (R. Amal).

the nature of the intermediate products that are formed and identify the points at which they occur during the reaction. The aim of the work is to link mechanistic insights to reaction kinetics.

2. Experimental

2.1. Catalyst and chemicals

TiO₂ Degussa P25 (primary particle size ~25–30 nm, surface area ~50 m² g⁻¹, anatase to rutile ratio of 4:1) was used as the photocatalyst. Malic acid was purchased from Sigma–Aldrich® with high purity (DL-Malic acid, 99%) and used as received. Perchloric acid (70%, Frederic Chemical Co.), malonic acid (99%, Sigma–Aldrich®), acetic acid (>99%, Ajax), sodium dihydrogen phosphate (M&B) and phosphoric acid (85%, Fluka) were analytical or HPLC grades and used without further purification. Ultra pure water, with a resistivity >18 M Ω⁻¹ cm⁻¹ at 298 K, from a Millipore Milli-Q water purification system was used to prepare all solutions.

2.2. Photocatalytic activity studies

Photocatalytic activity studies were performed in a 250 mL, spiral-type photoreactor as described by Coleman et al. [14]. A 0.2 g L⁻¹ TiO₂ suspension was prepared by dispersing a pre-determined weight of TiO₂ in water for 15 min in an ultrasonic bath (Unisonics). The initial pH of the TiO₂ suspension was adjusted to 3 ± 0.05 using 1 M perchloric acid solution. The suspension was illuminated for 30 min prior to the organic substrate addition to remove organic impurities in the system. An 18W black light blue lamp with maximum emission of 365 nm was used as the light source. The light was turned off and the system was air-equilibrated. 100 μL of malic acid solution, containing 2000 μg carbon, was then injected into the system. Dark adsorption of malic acid onto the photocatalyst was attained by circulating the suspension at a flow rate of 8 mL s⁻¹ through the photoreactor, for 20 min. When the system was illuminated and the photocatalytic reaction initiated, generated carbon dioxide was detected by an online conductivity meter (Jenway 4330). All experiments were conducted at ambient temperature and pressure.

2.3. Analytical methods

HPLC (Waters 2695) was used to identify organic compounds in the solution as the reaction progressed. The concentration of each organic compound was measured by its maximum absorbance wavelengths using a Photodiode Array Detector (PDA, Waters 2996). A reverse phase Atlantis T3 column (5 μm, 4.6 mm × 250 mm) was used to separate the compounds at 303 K. Sodium dihydrogen phosphate was used as the mobile phase and the pH was adjusted to 2.7 using phosphoric acid. The separation was performed under an isocratic condition with a mobile phase flow rate of 0.5 mL min⁻¹. Intermediate products were identified by comparing the retention times and spectra with those of pure standards. Standard solutions were used to develop external calibration curves for the quantification purposes, except for malonaldehydic acid which was not commercially available in a standard form. Samples (1.5 mL) were withdrawn regularly from the injection port and filtered through a 0.45 μm membrane filter prior to analysis.

Total organic carbon (TOC) analysis involved sampling from the photoreactor at selected intervals during the reaction and filtering through a 0.45 μm membrane filter prior to analysis. TOC content was determined using a Shimadzu TOC-V_{CSH} equipped with a non-dispersive infrared (NDIR) detector. The TOC was obtained by subtracting the inorganic carbon component from the total measured carbon.

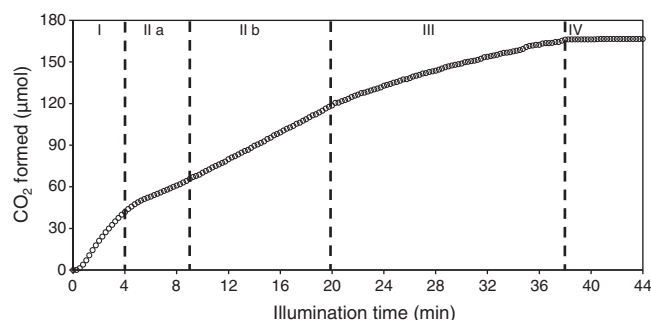


Fig. 1. Photomineralization profile of malic acid in a TiO₂ suspension using a spiral, slurry-type reactor. Initial experimental conditions: TiO₂ concentration: 0.2 g L⁻¹; malic acid: 2000 μg C; pH: 3 ± 0.05.

FTIR analysis was performed on a Nicolet Avatar 320. Prior to analysis, the particles were recovered by centrifuging the suspension and dried in a desiccator at room temperature for 2 days. Spectra were recorded over a mid-infrared range of 1200–3200 cm⁻¹ with a resolution of 4 cm⁻¹ and 200 scans. The spectra were taken using the software Omnic version 6.1a.

Zeta potential was used to monitor the presence of surface organics on the TiO₂ as the reaction proceeded. Samples (2 mL) were taken from the reactor at selected time intervals and measured using a Brookhaven ZetaPALS analyzer. TiO₂ zeta potential was also measured in the absence of malic acid to assess the effect of illumination on zeta potential of the photocatalyst.

2.4. Dark adsorption experiments

The dark adsorption studies of malic acid, malonic acid and acetic acid onto TiO₂ were performed in a 250 mL glass bottle at room temperature using a 0.2 g L⁻¹ TiO₂ suspension at pH 3 ± 0.05. The initial organic compound concentration was set at 2000 μg of carbon. The suspension was magnetically stirred with samples collected at selected intervals and assessed using HPLC and zeta potential analyses.

3. Results and discussion

3.1. Photocatalytic degradation of malic acid

Fig. 1 shows the rate of carbon oxidized with time following illumination of malic acid in the presence of the TiO₂ suspension. The experiment was repeated three times with good reproducibility. Malic acid photolysis was not observed in the absence of TiO₂ under illumination nor was it catalytically degraded in the presence of TiO₂ without illumination (data not shown).

During degradation, the mass of carbon oxidized increased with reaction time, and after approximately 38 min, 2000 μg C had been oxidized representing complete mineralization (equivalent to 167 μmol CO₂ formed). Also apparent in the mineralization profile are regions where the CO₂ generation rate varied as the reaction proceeded. Based on the rate changes, the mineralization profile has been divided into four distinct regions (I, II (a, b), III, and IV) as illustrated in Fig. 1 where: region I encompasses the initial degradation rate; region II (a, b) represents the degradation rate between 4 and 20 min; region III covers the degradation rate between 20 and 38 min and; region IV shows where complete mineralization has been achieved.

The parent and intermediate species generated and consumed as the photocatalytic degradation proceeded are given in Fig. 2. As seen in Fig. 2, three intermediate products were detected by HPLC as the reaction progressed. Malonic acid and acetic acid were confirmed by comparison with pure standards. An intermediate

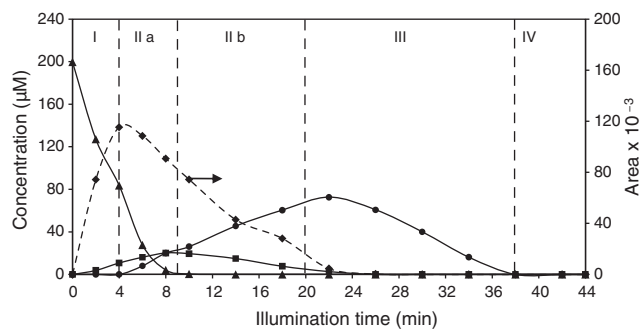


Fig. 2. Malic acid and the intermediate product profiles during malic acid photodegradation. (▲) Malic acid, (◆) Intermediate 1, believed to be malonaldehydic acid, (■) malonic acid, and (●) acetic acid.

(Intermediate 1) was also observed but its identity could not be positively confirmed on comparison with the available standards. It is believed that this intermediate is malonaldehydic acid based on the mechanistic pathways for malic acid photodegradation as described by Herrmann et al. [12] and its higher polarity from the HPLC profiles (Supplementary data, Fig. S1) when compared with malic acid. Consequently, as Intermediate 1 could not be confirmed with a commercial standard, its profile has been presented as the peak area from the HPLC analysis. The HPLC results show that malic acid is removed within the first 8 min, while Intermediate 1 and malonic acid began to form immediately upon illumination. The concentration of both Intermediate 1 and malonic acid continued to increase in the solution, reaching a maximum after 4 min and 9 min, respectively. This indicates that the degradation of both these compounds during this stage was slower than their formation. It is only when the malic acid is fully removed from the system (at 9 min) that the malonic acid begins to decline. This may be indicative of competitive adsorption between malic acid and malonic acid, with the adsorption of malic acid being favored. However, due to the error associated with dark adsorption measurements (Fig. 3) this could not be confirmed. Both malonic acid and Intermediate 1 were present in the system up to 22 min following illumination. Acetic acid began to form after 4 min and was persistent in the system until the 36th minute.

Based on the HPLC results, and comparing with Fig. 1, region II (in Fig. 1) can be further subdivided into two regions (IIa and IIb) where the first rate change (at 4 min) occurs when Intermediate 1 reaches a maximum, and the second rate change occurs when malonic acid reaches a maximum (9 min). This also corresponds to the point of complete malic acid consumption. The third rate change (at approximately 20 min) corresponds to when acetic acid reaches a maximum (and malonaldehydic acid has disappeared) while the

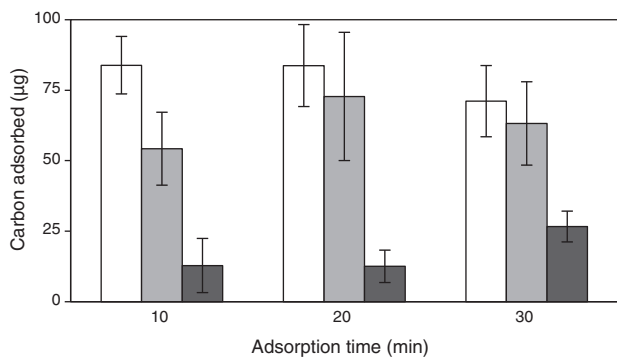


Fig. 3. The extent of carbon adsorbed onto the TiO₂ particles as (□) malic acid, (■) malonic acid, and (●) acetic acid in the absence of light. Initial experimental conditions: TiO₂ concentration: 0.2 g L⁻¹; organic loading: 2000 µg C; pH: 3 ± 0.05.

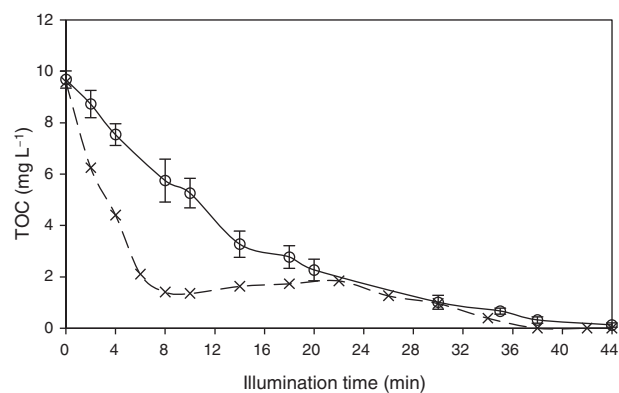
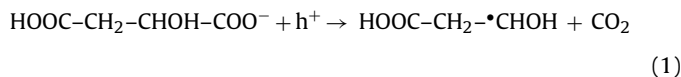


Fig. 4. TOC profiles during malic acid photodegradation. (○) TOC of samples; (×) TOC of malic acid and the intermediates.

fourth represents complete mineralization and corresponds to the consumption of all acetic acid. The TOC remaining in solution, as malic acid was photocatalytically degraded is presented in Fig. 4. As the reaction progressed, the TOC decreased and after 44 min of reaction, the final TOC was 0.1 mg L⁻¹, which corresponds to a total organic carbon removal of 99.9%. As seen in Fig. 4, the detectable TOC in solution differs with the TOC of malic acid and its intermediates obtained from HPLC analysis. The difference in the profiles was predominantly attributed to Intermediate 1 which could not be positively identified in the present study.

The oxidative photodegradation involves two strong oxidizing agents: photoholes (h⁺) and •OH. It is generally accepted that the photocatalytic degradation of malic acid is initiated by the photo-Kolbe reaction [15] as the adsorbed species has a higher probability of being attacked by photogenerated holes in shallow traps of the valence band of the photocatalyst [16,17]. Consequently, carbon dioxide is evolved and a carbon-centred radical is formed (reaction (1)):

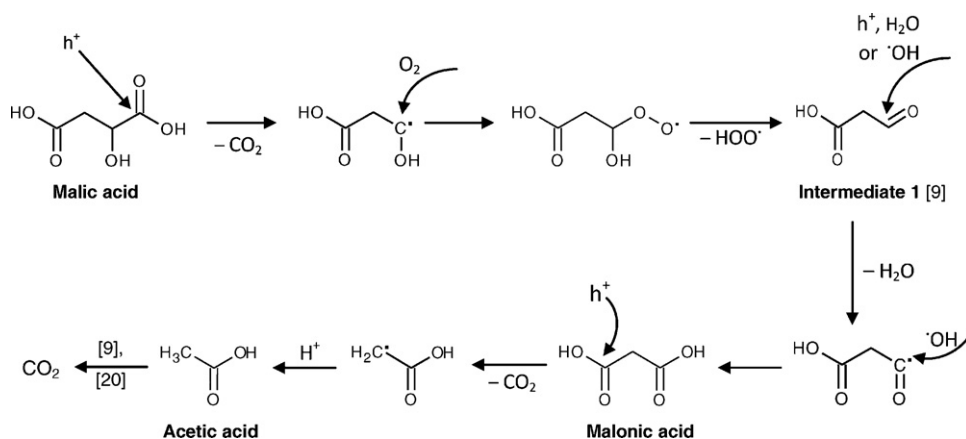


and oxygen is likely to give an aldehyde via reaction (2):



The photoholes and •OH continue the reaction and form the intermediate as shown in Fig. 2 with the consecutive formation reactions described in Scheme 1. Figs. 1 and 2 demonstrate that the decarboxylation of malic acid is a comparatively rapid process. The initial rapid generation of CO₂ is attributed to this process whereby within 4 min ~25% of the malic acid has been adsorbed and decarboxylated, predominantly forming Intermediate 1 plus traces of other intermediates such as malonic acid. It is anticipated that most of the carbon dioxide derived from this initial decarboxylation step and suggests that the malic acid decarboxylation reaction is preferred over subsequent photocatalytic steps in the degradation mechanism. Carboxylic acids are known to adsorb well onto the TiO₂ surface, particularly at low pH, as the acids are in their dissociated forms within this pH range and the TiO₂ surface is positively charged [5,18–20]. The extent of adsorption is depicted in Fig. 3 where ~80 ± 12 µg C, in the form of malic acid, is adsorbed on TiO₂ at pH 3.0 ± 0.05.

The onset of decline in Intermediate 1 represents the beginning of stage II and is characterized by a substantial decrease in the mineralization rate. This indicates that the degradation of Intermediate 1 is more arduous than malic acid. We suggest that the preferential adsorption of malic acid delayed the degradation of this intermediate in the system. The malonic acid concentration also continues



Scheme 1. Simplified mechanistic pathway for malic acid photodegradation by TiO₂ at reaction pH 3.

to increase. Malonic acid is believed to form by the H atom abstraction and the $\bullet\text{OH}$ addition to the aldehyde group of Intermediate 1 (see Scheme 1). The peak maxima for malonic acid occurs ~ 5 min after the maxima for Intermediate 1 (Fig. 2) and this is congruent with an upturn in the mineralization rate profile. As mentioned earlier, stage II was subdivided into regions IIa and IIb to convey this observation. We postulate that stage II represents the overall decarboxylation of the C₃ carbon chain with the sub-groups suggesting hydroxylation of the anticipated aldehyde group in Intermediate 1. The malonic peak maximum also coincides with the disappearance of malic acid. Furthermore, stage II covers the region where acetic acid is initially detected to when it reaches its maximum concentration in the system. The point where acetic acid reaches its maxima also corresponds to the point where Intermediate 1 and malonic acid reach negligible concentrations. Malonic acid photodegradation is believed to occur via the photo-Kolbe process, leading to decarboxylation of the C₃ chain and creating the acetate radical ($\bullet\text{CH}_2\text{COOH}$ – Scheme 1). This carbon-centred radical may then react with $\bullet\text{OH}$ to yield glycolic acid and/or generate acetic acid via the H addition [21]. As acetic acid was observed during degradation, but not glycolic acid, this suggests that the H addition to the acetate radical was favored in our system. Overall, it appears that the mineralization rate for stage II is dominated by the decarboxylation of Intermediate 1 to form acetic acid with an initial hindrance due to the increasing presence of malonic acid.

Stage III is marked by a decrease in the mineralization rate (Fig. 1) and encompasses the decrease in acetic acid concentration in the solution. Peroxyl radicals are known to react with the acetate radical to form oxalic acid as was reported by Dolamic and Bürgi [22]. Dolamic and Bürgi found oxalic acid to be the major intermediate product during malonic acid mineralization in a small volume flow-through cell [22]. Alternatively, the acetic acid may undergo a sequence of reactions with photogenerated $\bullet\text{OH}$ in solution leading to its mineralization [23]. The comparatively slow mineralization rate encountered for acetic acid is typical of this molecule and has been described by others [24,25]. This stems from the natural refractory characteristic of acetic acid [26,27]. Moreover, as demonstrated in Fig. 3, acetic acid is poorly adsorbed on the TiO₂ surface under the reaction conditions. This may contribute to its slower rate of degradation and suggests its photooxidation mechanism may be dominated by $\bullet\text{OH}$ attack in solution [16]. Its slower degradation rate may also account for the lack of observed intermediates (e.g. oxalic acid, formic acid, and formaldehyde [12]) in solution as the rate of intermediate consumption may be higher than their generation rate [28]. Additionally, the greater adsorption of such intermediates onto the TiO₂ surface [29–31] means such compounds would be present in solution only in negligible, unde-

tectable amounts. The TOC results (presented in Fig. 4) show that intermediates were still being mineralized while these compounds were no longer being detected by HPLC. In a separate experiment (not shown), acetic acid was photodegraded under the same conditions as used for malic acid degradation, with no intermediates detected by HPLC, despite its complete mineralization.

Stage IV represents the completion of malic acid photodegradation as well as its intermediates. Confirmation of complete mineralization of all the carbon is demonstrated by the TOC results in Fig. 4, which show that after 44 min negligible organic carbon remained in the system.

3.2. Link between dark adsorption and photodegradation kinetics

Approximately 3.5% of malic acid was adsorbed at equilibrium under dark conditions. This corresponds to a surface coverage of about 0.5 molecules/nm². With this low surface coverage, its degradation kinetics fit the Langmuir–Hinshelwood model. At a low reactant concentration (<1 mM) the reaction obeys apparent first order reaction kinetics [1].

The pH of the system plays an important role in the dark adsorption of organics on the surface of TiO₂ as it governs the extent of the acid dissociation in water and the surface properties of TiO₂ [5,28,32,33]. The initial solution pH was maintained at 3 ± 0.05 with pH variation during the dark adsorption studies and photodegradation found to be negligible. The extent of dark adsorption is related to the acid dissociation constant (pK_a) as presented in Table 1 [34]. Under the same conditions, 25.8% of malic acid will be in dissociated form as $\text{HOOC-CH}_2\text{-CHOH-COO}^-$ and 0.2% in the form of $^- \text{OOC-CH}_2\text{-CHOH-COO}^-$. This dissociation level can explain its strong adsorption as observed in Fig. 3. In the instance of malonic acid, which has pK_a values of 2.83 and 5.7, 59.9% will be dissociated as $\text{HOOC-CH}_2\text{-COO}^-$ and 0.1% in the form of $^- \text{OOC-CH}_2\text{-COO}^-$. Acetic acid has a pK_a value of 4.76 whereby, at $\text{pH } 3 \pm 0.05$, only 1.7% of acetic acid exists in ionic form. In comparison to malic and malonic acids, acetic acid adsorbed least on the TiO₂ surface. The dark adsorption studies support the photo-Kolbe reaction dominated mechanism for malic acid and malonic acid given their greater

Table 1
 pK_a values of parent and intermediate carboxylic acids in water at 25 °C [34].

Substance	Structural formula	pK_{a1}	pK_{a2}
DL-Malic acid ^a	$\text{HOOC-CH}_2\text{-CHOH-COOH}$	3.46	5.10
Malonic acid	$\text{HOOC-CH}_2\text{-COOH}$	2.83	5.70
Acetic acid	HOOC-CH_3	4.76	–
Oxalic acid	HOOC-COOH	1.27	4.27

^a D-(+), or dextromalic acid; L-(–), or levomalic acid.

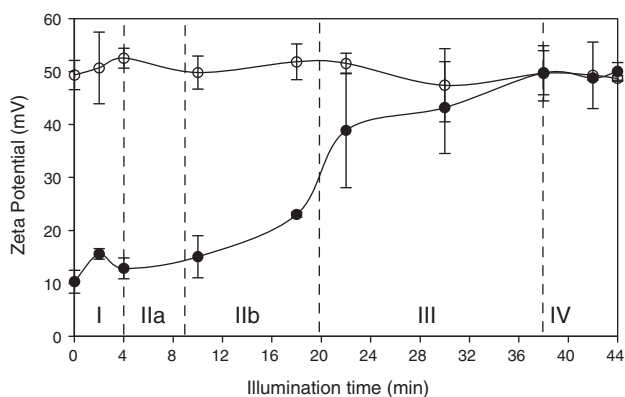


Fig. 5. Change in the zeta potential of (○) illuminated aqueous TiO₂ suspension and (●) illuminated reaction mixture/TiO₂ suspension.

degree of adsorption. The dark adsorption studies on acetic acid suggest •OH are mostly likely responsible for degrading this compound in solution, which is believed to be a slower process. This is also reflected in the HPLC and photodegradation results presented in Figs. 1 and 2, respectively. Included in Table 1 is the pK_a of oxalic acid (pK_{a1} = 1.27; pK_{a2} = 4.27) supporting its anticipated high adsorption on the TiO₂ surface at pH 3.

During degradation, the ionic strength is important in adsorption/desorption reaction which affects the surface charge of the photocatalyst. However the initial reaction pH was adjusted to 3 ± 0.05 (1 mM), and the pH did not significantly vary greatly as the reaction proceeded (the pH change was measured to be 0.05 during the course of the experiment). Coupled with the low initial concentration of malic acid (0.2 mM), the total ion concentration in solution (ionic strength) is not expected to vary greatly during the reaction. Therefore, in this study a change in the ionic concentration is not expected to greatly affect adsorption/desorption kinetics or reaction kinetics.

3.3. TiO₂ zeta potential during photodegradation

Zeta potential has been demonstrated as an appropriate tool to study interactions between organic compounds and the TiO₂ surface in the bulk phase [35]. In the present study, the initial negative shift in TiO₂ zeta potential in the presence of an organic indicates its adsorption on the particle surface. A higher concentration of dissociated organic in solution promotes greater adsorption of the organic on the TiO₂ surface, neutralizing the positive charge of the TiO₂, and consequently lowering the zeta potential value. Zeta potential of the TiO₂ photocatalyst was measured during the malic acid photodegradation and as can be seen in Fig. 5, shifts in zeta potential were apparent during the reaction.

As seen in Fig. 5, the zeta potential of illuminated TiO₂ in the absence of organic compounds remained at a constant value of around +50 mV, which is similar to the value reported by others [35]. The presence of malic acid in the solution decreased TiO₂ zeta potential to ~+10 mV, clearly indicating adsorption of this acid on the TiO₂ surface. Upon illumination, the zeta potential remained relatively constant at +10 mV until 10 min after which it began to increase. An illumination time of 10 min correlates with the point at which all malic acid was removed from the system and the malonic acid reached its maximum concentration (Fig. 2). Zeta potential values for malic and malonic acids adsorbed in the absence of light (Fig. 6) again demonstrate their capacity for adsorption and support the decrease in zeta potential seen in Fig. 5. Over the 10–20 min period, there is a mild increase in zeta potential to ~+20 mV. At this point a rapid step-up in the value is observed. The step-up coincides with malonic acid removal and the acetic acid maxima in Fig. 2 and

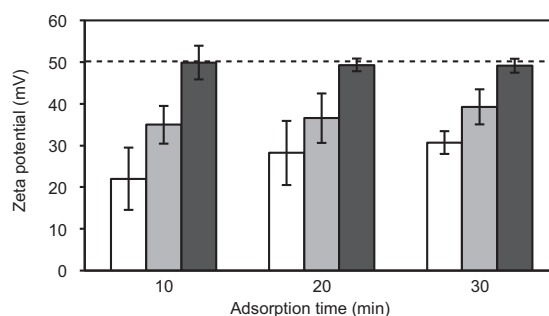


Fig. 6. The influence of (□) malic acid, (▤) malonic acid, and (■) acetic acid adsorption on TiO₂ zeta potential in the absence of light. (—) The average zeta potential of pure TiO₂ without any organics present. Initial experimental conditions: TiO₂ concentration: 0.2 g L⁻¹; organic loading: 2000 μg C; pH: 3 ± 0.05.

may be explained by the negligible influence acetic acid has on TiO₂ zeta potential (Fig. 6). The divergence in zeta potential values beyond 24 min may be indicative of other adsorbed species on the surface (e.g. oxalic acid, formic acid, formaldehyde) but errors associated with these values make confirmation difficult. Oxalic and formic acids, when adsorbed onto the TiO₂ surface, lead to a lowering of the TiO₂ zeta potential [20,35] although, due to the fast dynamics of their degradation, a shift in the zeta potential may not be observable. Lam et al. [35] postulated that the fast disappearance of intermediates such as formaldehyde and formic acid during methanol photooxidation was the reason behind the zeta potential of TiO₂ being unaffected as the reaction proceeded. By 38 min the zeta potential has returned to the neat TiO₂ value indicating organics are no longer adsorbed on the surface.

3.4. FTIR analysis during malic acid photodegradation

Fig. 7 provides the infrared spectra of bare TiO₂, malic acid/TiO₂ (t = 0) and reaction mixture/TiO₂ under illumination. In the instance of bare TiO₂, the band at 1633 cm⁻¹ is due to the deformation vibrations of H₂O (δ_{H₂O}) and the C=O stretch of CO₂ present in the system [33]. For malic acid/TiO₂ (t = 0 min), small features between 2960 and 2895 cm⁻¹ correlate with the CH₂ asymmetric and symmetric stretch. Bands around 1380 and 1260 cm⁻¹ are assigned to C–H and CH₂ deformation vibrations of malic acid. Signals due to the stretching of carbonyl groups ν(C=O) are expected at (1650–1800 cm⁻¹) and signals of ν(C–O) are expected at 1270–1450 cm⁻¹. The stretching of C–C mode and O–H deformation vibrations of carboxylic acids are expected at 1380–1280 cm⁻¹ [36,37].

Firstly, it is clear a number of the signals overlap. Secondly, the H₂O band at 1633 cm⁻¹ overlaps and overwhelms some of the signals of interest and highlights the problems associated with using FTIR (alone) to study adsorbed intermediates on the TiO₂ surface. Despite this interference, changes in the FTIR spectra after illumination of reaction mixture/TiO₂ samples may still reveal information regarding the degradation and formation of strongly adsorbed species as the reaction proceeds, as highlighted in the ensuing discussion.

After 4 min illumination (beginning of stage II in Fig. 1), strong bands appeared at 2960 and 2918 cm⁻¹. This indicates that the dominant adsorbed species contain CH and/or CH₂ in their carbon chain. The presence of a new band at 2850 cm⁻¹ was also observed. As the C–H stretch and deformation vibrations of an aliphatic aldehyde are typically observed at 2900–2800 cm⁻¹ and 1440–1325 cm⁻¹, respectively [37], this may indicate the increase in an adsorbed aldehyde-containing intermediate on the TiO₂ surface from decarboxylation of the parent acid substituted with one hydroxyl group [38].

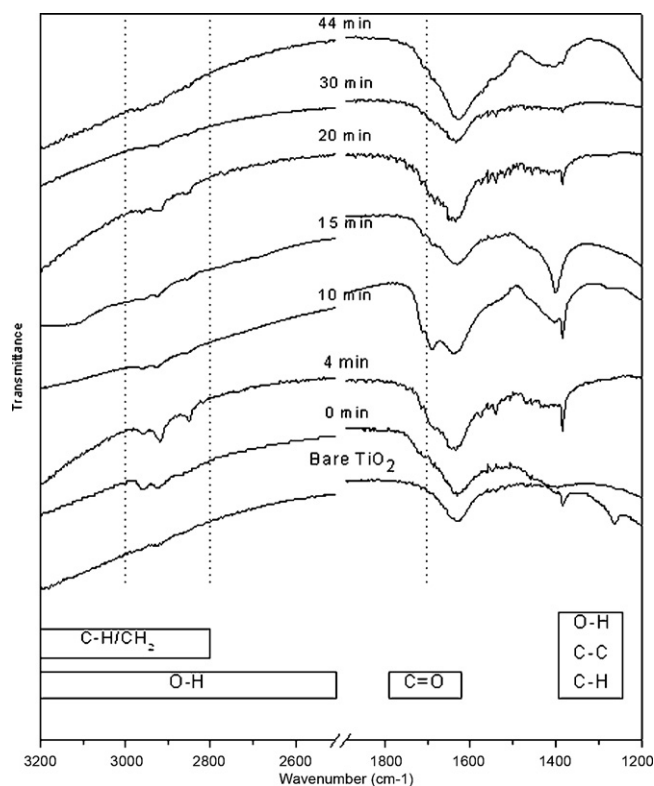


Fig. 7. Infrared spectra of bare TiO₂, malic acid/TiO₂ and reaction mixture/TiO₂ taken at different illumination times. Note: $t = 0$ min indicates the time prior to UV light illumination (i.e. the malic acid/TiO₂ system).

As the reaction progressed, the intensity of $\nu(\text{CH}$ and $\text{CH}_2)$ decreased. This could indicate degradation or desorption of this species. At 10 min of reaction time, a strong shoulder around 1700 cm^{-1} evolved, and could be due to a $\text{C}=\text{O}$ stretch, suggesting $\text{C}=\text{O}$ -containing species were strongly adsorbed onto the TiO₂ surface. The compound could be oxalic and/or formic acid as these species are suspected as strongly adsorbing intermediates [18,22,31,39,40]. After 20 min illumination (stage III in Fig. 1), a small band at 2850 cm^{-1} appeared which again indicates the adsorbed intermediate is dominated by a $\text{C}-\text{H}$ group. This could be an aldehyde-containing species such as glyoxylic acid and/or formaldehyde generated during acetic acid degradation [12]. By the end of the reaction ($t = 44$ min), the spectra is similar to bare TiO₂ with a small band around 1400 cm^{-1} . This band may be assigned to a $\text{C}-\text{O}$ stretch which could be indicative of carbonate species ($1605\text{--}1320\text{ cm}^{-1}$ [37,39]) generated during the degradation, while the $\nu(\text{C}=\text{O})$ of this species overlies the H_2O band.

Scheme 1 summarises the reaction mechanism of the photocatalytic degradation of malic acid over TiO₂. It is based on the observations and analyses presented in our study. Not all the possible intermediates could be identified in this work with gaps in the mechanism filled by pathways developed by other groups who have studied malic acid degradation and reported other intermediates in addition to the ones detected in our system [12,13]. Different reaction parameters such as light intensity and reactant concentrations could contribute to the differences in intermediates detected in this and their systems. Herrmann et al. [12] detected malonaldehydic acid as the main intermediate in addition to malonic, acetic, formic, fumaric/maleic, tartaric, tartronic, glycolic, oxalic, lactic and pyruvic acids, and acetaldehyde, mostly in trace amounts. On the other hand, Danion et al. [13] detected malonic acid as the primary intermediate, together with tartaric, fumaric, maleic, pyruvic and oxalacetic acids. In their systems, the reaction solu-

tion pH was neutral, which is distinctly different to the acidic pH ($\text{pH} = 3$) of the system studied here. The higher pH is expected to promote $\bullet\text{OH}$ driven oxidation pathways and thus promote the formation of pyruvic acid for example, which was not observed in our system. Moreover, the surface coverage of the substrate on the photocatalyst surface influences the initial degradation rate. In the systems studied by Herrmann et al. [12] and Danion et al. [13], the surface coverage of malic acid was 1.2 and 4.6 molecules/ nm^2 , respectively. A higher surface coverage leads to faster degradation rates. It also increases the probability of malic acid being degraded via the photo-Kolbe reaction and via $\bullet\text{OH}$ attack. It is suspected that the difference in surface coverage is responsible for the different intermediates detected by [12,13], compared to our system. In the generalized mechanistic approach presented here, key steps are identified, and hindering steps are highlighted. Based on our observations, it seems that rate changes are strongly influenced by the extent of intermediate adsorption on the TiO₂ surface. Competitive adsorption could be the key in determining favored pathways with further studies needed to confirm this.

4. Conclusions

The photocatalytic degradation of malic acid showed a mineralization profile possessing varying mineralization rates. The mineralization rates changed depending on the dominant intermediate present in the solution. The initial mineralization stage was fast ($\sim 175\text{ }\mu\text{g C/min}$) and is believed to be due to the fast mineralization of strongly adsorbed malic acid via a photo-Kolbe mechanism. The second stage of mineralization was represented by a slowing of the CO_2 generation rate ($\sim 50\text{--}70\text{ }\mu\text{g C/min}$) with the continued degradation of an unidentified intermediate (believed to be malonaldehydic acid), the continued formation of malonic acid and the onset of acetic acid formation. During the third stage of mineralization, the rate decreased further ($\sim 30\text{ }\mu\text{g C/min}$), coinciding with a build up of acetic acid in the solution. Based on photocatalytic mineralization results, dark adsorption studies, FTIR and zeta potential results, it appears that the affinity of intermediates for the TiO₂ surface together with their structure affects the reaction mineralization kinetics.

Acknowledgements

The authors would like to thank the Australian Research Council (ARC) Centre of Excellence for Functional Nanomaterials for financially supporting this work and the Australian Development Scholarship (ADS) program for funding W. Irawaty's scholarship.

Appendix A. Supplementary data

Supplementary data associated with this article can be found, in the online version, at doi:10.1016/j.molcata.2010.11.027.

References

- [1] J.-M. Herrmann, Catal. Today 53 (1999) 115–129.
- [2] M.A. Fox, M.T. Dulay, Chem. Rev. 93 (1993) 341–357.
- [3] M.R. Hoffmann, S.T. Martin, W. Choi, D.W. Bahnemann, Chem. Rev. 95 (1995) 69–96.
- [4] O. Legrini, E. Oliveros, A.M. Braun, Chem. Rev. 93 (1993) 671–698.
- [5] M.I. Franch, J.A. Ayllón, J. Peral, X. Domènech, Catal. Today 76 (2002) 221–233.
- [6] M.I. Franch, J.A. Ayllón, J. Peral, X. Domènech, Appl. Catal. B 50 (2004) 89–99.
- [7] Y.-C. Chan, J.-N. Chen, M.-C. Lu, Chemosphere 45 (2001) 29–35.
- [8] D. Friedmann, C. Mendive, D. Bahnemann, Appl. Catal. B 99 (2010) 398–406.
- [9] F. Denny, J. Scott, K. Chiang, W.Y. Teoh, R. Amal, J. Mol. Catal. A: Chem. 263 (2007) 93–102.
- [10] S.S. Watson, D. Beydoun, J.A. Scott, R. Amal, Chem. Eng. J. 95 (2003) 213–220.
- [11] F. Denny, J. Scott, V. Pareek, G.D. Peng, R. Amal, Chem. Eng. Sci. 64 (2009) 1695–1706.
- [12] J.-M. Herrmann, H. Tahiri, C. Guillard, P. Pichat, Catal. Today 54 (1999) 131–141.

- [13] A. Danion, J. Disdier, C. Guillard, N. Jaffrezic-Renault, J. Photochem. Photobiol. A 190 (2007) 135–140.
- [14] H.M. Coleman, C.P. Marquis, J.A. Scott, S.-S. Chin, R. Amal, Chem. Eng. J. 113 (2005) 55–63.
- [15] B. Kraeutler, A.J. Bard, J. Am. Chem. Soc. 100 (1978) 5985–5992.
- [16] K. Chiang, T.M. Lim, L. Tsen, C.C. Lee, Appl. Catal. A 261 (2004) 225–237.
- [17] D.W. Bahnemann, M. Hilgendorff, R. Memming, J. Phys. Chem. B 101 (1997) 4265–4275.
- [18] U. Diebold, Surf. Sci. Rep. 48 (2003) 53–229.
- [19] J. Araña, J.M.D. Rodríguez, O.G. Díaz, J.A.H. Melián, J.P. Peña, Appl. Sci. 252 (2006) 8193–8202.
- [20] H. Tran, J. Scott, K. Chiang, R. Amal, J. Photochem. Photobiol. A 183 (2006) 41–52.
- [21] Y. Inel, A.N. Ökte, J. Photochem. Photobiol. A 96 (1996) 175–180.
- [22] I. Dolamic, T. Bürgi, J. Phys. Chem. B 110 (2006) 14898–14904.
- [23] Y. Nosaka, K. Koenuma, K. Ushida, A. Kira, Langmuir 12 (1996) 736–738.
- [24] Leitner tp:ag N.K.V., M. Doré, Water Res. 31 (1997) 1383–1397.
- [25] M.A. Oturan, M. Pimentel, N. Oturan, I. Sirés, Electrochim. Acta 54 (2008) 173–182.
- [26] A. Sinha, S. Chakrabarti, B. Chaudhuri, S. Bhattacharjee, P. Ray, Ind. Eng. Chem. Res. 46 (2007) 3101–3107.
- [27] Y. Ogata, K. Tomizawa, K. Takagi, Can. J. Chem. 59 (1980) 14–18.
- [28] N. Serpone, J. Martin, S. Horikoshi, H. Hidaka, J. Photochem. Photobiol. A 169 (2005) 235–251.
- [29] K.D. Dobson, A.J. McQuillan, Spectrochim. Acta A 55 (1999) 1395–1405.
- [30] T. Lana-Villarreal, J.M. Pérez, R. Gómez, C. R. Chim. 9 (2006) 806–816.
- [31] A. Vittadini, A. Selloni, F.P. Rotzinger, M. Grätzel, J. Phys. Chem. B 104 (2000) 1300–1306.
- [32] H. Harada, T. Ueda, J. Phys. Chem. 93 (1989) 1542–1548.
- [33] Q. Chen, J.M. Song, F. Pan, F.L. Xia, J.Y. Yuan, Environ. Technol. 30 (2009) 1103–1109.
- [34] G.W. Gokel, Dean's Handbook of Organic Chemistry, second ed., McGraw-Hill, New York, 2004.
- [35] S.W. Lam, K. Chiang, T.M. Lim, R. Amal, G.K.-C. Low, J. Photochem. Photobiol. A 187 (2007) 127–132.
- [36] J.-J. Max, C. Chapados, J. Phys. Chem. A 106 (2002) 6452–6461.
- [37] G. Socrates, Infrared and Raman Characteristic Group Frequencies: Tables and Charts, third ed., John Wiley & Sons, Chichester, 2001.
- [38] N.K.V. Leitner, M. Dore, J. Photochem. Photobiol. A 99 (1996) 137–143.
- [39] I. Dolamic, T. Bürgi, J. Catal. 248 (2007) 268–276.
- [40] F.P. Rotzinger, J.M. Kesselman-Truttman, S.J. Hug, V. Shklover, M. Grätzel, J. Phys. Chem. B 108 (2004) 5004–5017.